Crystal structures and electrochemical properties of two phases of tetrabutylammonium bis(1,3-dithiole-2-thione-4,5-diselenolato)-nickelate(III)

J. P. Cornelissen, J. G. Haasnoot*, J. Reedijk
Department of Chemistry, Gorlaeus Laboratories, Leiden University, P.O. Box 9502, 2300 RA Leiden, (Netherlands)

C. Faulmann, J.-P. Legros, P. Cassoux
Laboratoire de Chimie de Coordination du CNRS, associé à l'Université Paul Sabatier, 205 Route de Narbonne, 31077 Toulouse Cédex (France)

and P. J. Nigrey
Sandia National Laboratories, Department 6642, Albuquerque, NM 87185-5800 (USA)

(Received May 29, 1992)

Abstract

The crystal structures of two phases (α and β) of $[Bu_4N]_2[Ni(dsit)_2]_2$ are reported (dsit = 1,3-dithiole-2-thione-4,5-selenolate). The compound crystallises either in blocks (α-phase) or needles (β-phase). The α-phase crystallises in the triclinic space group $P\bar{1}$, with $a = 12.381(3)$, $b = 14.009(2)$, $c = 9.571(1)$ Å, $\alpha = 94.43(1)$, $\beta = 99.61(2)$, $\gamma = 81.32(2)°$ and $Z = 1$ with the asymmetric unit having the formula $Ni_2C_{44}H_{72}N_2S_{12}Se_8$. The β-phase crystallises in the triclinic space group $P\bar{1}$, with $a = 11.820(1)$, $b = 14.998(1)$, $c = 9.517(1)$ Å, $\alpha = 96.980(8)$, $\beta = 100.251(9)$, $\gamma = 76.926(8)°$ and $Z = 1$ with the asymmetric unit having the formula $Ni_2C_{44}H_{72}N_2S_{12}Se_8$. The structures were solved by direct methods, and refined by Fourier and least-squares techniques. Both crystal structures differ only marginally. They consist of anionic dimers made up of two chemically bound $Ni(dsit)_2$ units. The Ni atom is square pyramidally coordinated by five selenium donor atoms, with the apically bridging Ni–Se distances (2.48 and 2.47 Å for α-$[Bu_4N]_2[Ni(dsit)_2]_2$ and β-$[Bu_4N]_2[Ni(dsit)_2]_2$, respectively) being significantly longer than the equatorial distances (2.316–2.347 Å). In the β-phase one of the thionyl groups and three of the four butyl chains of the cations are in disorder. Because of the bulky nature of the cations, no short interdimer contacts are present in the lattices. Cyclic voltammetry studies of $[Bu_4N]_2[Ni(dsit)_2]_2$ in acetone show a first reversible $2[Ni(dsit)_2]^- \rightleftharpoons [Ni(dsit)_2]_2^{2-}$ couple at $E_{1/2} = -0.12$ V (versus Ag/AgCl), and a second quasi-reversible couple involving a single anodic peak at 0.18 V and two reduction peaks at 0.08 and −0.01 V.

Introduction

The search for new molecular conductors has now led to more than 40 compounds which are able to undergo a transition to the superconducting state. To date, apart from the recently found fulleride salts [1], the highest T_cs belong to the members of the κ-(BEDT-TTF)$_2$X series, where the typical non-stacking arrangement of (BEDT-TTF)$_2$ dimers seems to be responsible for the existence of a truly multi-dimensional conduction pathway. More than ten different κ-type salts have been shown to be superconductors [2].

In contrast, so far only five superconductors based on a formally inorganic acceptor molecule, namely $M(dmit)_2^{2-}$ (where dmit = $C_3S_5^{2-}$ = 1,3-dithiole-2-thione-4,5-dithiolate) have been reported, i.e. [TTF][Ni(dmit)$_2$]$_2$, α-[TTF][Pd(dmit)$_2$]$_2$, β-[TTF][Pd(dmit)$_2$]$_2$, [Me$_4$N][Ni(dmit)$_2$]$_2$ [3] and, very recently, β-[Me$_4$N][Pd(dmit)$_2$]$_2$ [4]. Furthermore, all of these salts will only turn superconducting at high pressures, whereas for many of the (BEDT-TTF)$_2$X compounds no extra pressure is required to achieve superconductivity. The reason for fewer examples of superconductivity in M(dmit)$_2$ than in the organic radical BEDT-TTF seems to stem from the difference in planarity of both systems. This results in different molecular arrangements, which are often κ-type for BEDT-TTF and generally 1-D stacking for M(dmit)$_2$ systems. It is known from transfer-integral calculations that a compound which crystallises in such a 1-D or quasi-1-D stacking mode tends to show highly anisotropic conductivity [5]. Because of its

*Author to whom correspondence should be addressed.

0020-1693/92/$5.00

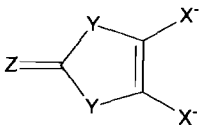

X = Y = Z = S dmit
X = Y = S, Z = Se dmise
X = Se, Y = Z = S dsit
X = Z = Se, Y = S dsise
X = Y = Z = Se dsis

Scheme 1.

lower dimensionality, conductors based on the $M(dmit)_2$ system are often susceptible to a lattice distortion in the stacking direction — the well-known Peierls distortion — which is observed as a change from metallic to semiconducting (or insulating) behaviour [6].

To study the possibilities of obtaining a multi-dimensional molecular arrangement of acceptor units, various selenium analogs of dmit have been prepared over the past few years (Scheme 1) [7–12]. Of these selenium-containing systems, the dsit ligand (where dsit = $C_3S_3Se_2^{2-}$ = 1,3-dithiole-2-thione-4,5-selenolate) is the most studied. So far, only $Ni(dsit)_2$ salts have been structurally characterised, and, apart from $[Bu_4N]_2[Ni(dsit)_2]$ [9], they all consist of tightly bound $[Ni(dsit)_2]_2$ dimers [10]. The only two known mixed-valence salts, $[Me_4N][Ni(dsit)_2]_2$ and $[Me_4P][Ni(dsit)_2]_2$, reported by Williams and co-workers show a high conductivity at room temperature, but they behave as semiconductors over the entire temperature range [11, 13]. Moreover, they possess a packing mode reminiscent of the superconducting κ-phase (BEDT-TTF)$_2$X salts. Therefore, $Ni(dsit)_2$ compounds may have the potential to form metallic, and even superconducting, solids.

The first two $Ni(dsit)_2$ salts of which the crystal structure was solved were $[Bu_4N]_2[Ni(dsit)_2]$ and $[Bu_4N]_2[Ni(dsit)_2]_2$ [9, 10]. However, no atomic coordinates were published. During our synthesis of $[Bu_4N]_2[Ni(dsit)_2]_2$, needed for the electrochemical preparation of mixed-valence salts, we discovered that in fact two phases of $[Bu_4N]_2]Ni(dsit)_2]_2$ can form. They are denoted hereafter as α-$[Bu_4N]_2[Ni(dsit)_2]_2$ and β-$[Bu_4N]_2[Ni(dsit)_2]_2$. The α-phase appears to be identical to the one previously reported [10]. In this paper both single crystal X-ray structures are fully described and compared to each other.

Experimental

Materials

Synthesis of red selenium

The synthesis of red selenium is based on the reduction of SeO_2 by the following reaction

$$SeO_2 + H_2NNH_2 \longrightarrow Se + 2H_2O + N_2$$

A solution of 11.1 g of SeO_2 in 150 ml water was cooled in an ice bath. A solution of 5 ml $H_2NNH_2 \cdot H_2O$ in 45 ml water was added dropwise over a period of *c.* 45 min while the reaction mixture was vigorously stirred and put under vacuum. Foaming occurred, and the red solid started to precipitate immediately [14]. It should be noted that the red modification is unstable in water and slowly forms black selenium upon standing. The product was filtrated, washed with water, alcohol and ether, and left drying in air. Yield 5.9 g (60%).

Synthesis of $[Bu_4N]_2[Ni(dsit)_2]$

The starting compound $[Bu_4N]_2[Ni(dsit)_2]$ was prepared according to the previously reported procedure [10] with the following alterations: instead of elemental black selenium the more active, red form of selenium (*vide supra*) was used. The $NiCl_2$ was added as a methanol solution. Elemental analyses were in agreement with the molecular formula $Ni_1C_{38}H_{72}N_2S_6Se_4$. Yield 55%.

Synthesis of α- and β-$[Bu_4N]_2[Ni(dsit)_2]_2$

$[Bu_4N]_2[Ni(dsit)_2]$ was oxidised to $[Bu_4N]_2[Ni(dsit)_2]_2$ by using a solution of I_2 in acetone as oxidising agent, according to the general recipe of Steimecke *et al.* [15]. The crude product was recrystallised from acetone/isopropanol, filtrated, washed with cold methanol and dried. Elemental analyses were in agreement with the molecular formula $Ni_2C_{44}H_{72}N_2S_{12}Se_8$. Yield 81%.

After recrystallisation black, chunky blocks, which proved to be α-$[Bu_4N]_2[Ni(dsit)_2]_2$, as well as black needles of the β-$[Bu_4N]_2[Ni(dsit)_2]_2$ phase were obtained together. A saturated solution of both forms in acetone yielded only crystals of the α-phase again, when allowed to evaporate in air. Therefore, the α-phase of $[Bu_4N]_2[Ni(dsit)_2]_2$ seems to be thermodynamically more stable than the β-form.

Cyclic voltammetry studies

All electrochemical measurements were performed by using a DACFAMOV 05-03 instrument [16, 17]. The electrochemical cell used for cyclic voltammetry employed a platinum working electrode, a platinum wire as the auxiliary electrode and a 0.1 N Ag/AgCl reference electrode. Measurements were carried out on acetone solutions containing 10^{-3} M $[Bu_4N]_2[Ni(dsit)_2]_2$, with use of 0.1 M Bu_4NPF_6 as the supporting electrolyte. Argon was passed through the

solution prior to taking the measurements and an argon blanket was maintained above the solution during experiments.

X-ray crystal structure determination

A representative crystal of each phase was selected and mounted on a CAD4 Enraf-Nonius diffractometer. Both crystals are triclinic (space group $P1$ or $P\bar{1}$). Unit-cell parameters were obtained from least-squares calculations based on the setting angles of 25 reflections in the 10–15° θ range for the α-phase, and 23 reflections in a 13–16° θ range for the β-phase. Intensity data were collected in the $\omega/2\theta$ scan mode up to a maximum θ angle of 25° for the α-phase and 22° for the β-phase (Mo Kα radiation, $\lambda = 0.71069$ Å). The intensity of three reflections was monitored throughout the data collection. No significant decay was observed. In both cases, empirical absorption correction was applied to the intensities. Crystal data, data collection and refinement parameters are summarized in Table 1.

For both structures, the metal atom, the selenium atoms and most of the sulfur atoms were located using the SHELX-76 package program [18]. The remaining non-hydrogen atoms were found by conventional difference Fourier calculations. The atomic parameters were refined by the full-matrix least-squares technique [19], assuming the centrosymmetric space group $P\bar{1}$ on the basis of intensity statistics. For the α-phase, all non-hydrogen atoms were refined with anisotropic thermal parameters. The β-phase shows some degree of disorder (*vide infra*). The disordered atoms (i.e. the terminal sulfur atom of one of the dsit ligands and the terminal carbon atom of three of the four butyl groups of the Bu_4N^+ cation) were considered statistically distributed (50%, 50%) over two positions and were refined isotropically. In order to keep the N_o/N_v ratio at a reasonable value, the carbon atoms of the dsit ligands and the cation were refined isotropically to reduce the number of refined parameters.

The contribution of the hydrogen atoms was computed using idealised, unrefined positions (d(C–H) = 0.95 Å) and arbitrary isotropic temperature factors. For the α-phase, all hydrogen atoms were included. For the β-phase, the hydrogens bonded to the disordered atoms were not included; the hydrogen atoms of the last-but-one CH_2 groups of the three disordered butyl chains were also omitted.

The final reliability indices and the values of the highest residual peaks in the final difference Fourier maps are given in Table 1. Final non-hydrogen atom positional and equivalent or isotropic thermal parameters are listed in Tables 2 and 3. The atomic numbering scheme for α-$[Bu_4N]_2[Ni(dmit)_2]_2$ and β-$[Bu_4N]_2[Ni(dmit)_2]_2$ is shown in Figs. 1 and 2. Atomic scattering

TABLE 1. Experimental data of single crystal X-ray diffraction studies for α-$[Bu_4N]_2[Ni(dsit)_2]_2$ and β-$[Bu_4N]_2[Ni(dsit)_2]_2$

Compound	α-$[Bu_4N]_2[Ni(dsit)_2]_2$	β-$[Bu_4N]_2[Ni(dsit)_2]_2$
Morphology	blocks	needles
Formula	$Ni_2C_{44}H_{72}N_2S_{12}Se_8$	$Ni_2C_{44}H_{72}N_2S_{12}Se_8$
M_r	1762.95	1762.95
Crystal system	triclinic	triclinic
Space group	$P\bar{1}$	$P\bar{1}$
a (Å)	12.381(3)	11.820(1)
b (Å)	14.009(2)	14.998(1)
c (Å)	9.571(1)	9.517(1)
α (°)	94.43(1)	96.980(8)
β (°)	99.61(2)	100.251(9)
γ (°)	81.32(2)	76.926(8)
Volume (Å^3)	1615.7(5)	1611.3(3)
Z	1	1
F(000)	870.00	870.00
D_c (g cm^{-3})	1.812	1.817
D_m (g cm^{-3})	1.82	1.82
λ(Mo Kα) (Å)	0.71069	0.71069
μ (cm^{-1})	54.5	54.7
Scan type	$\omega/2\theta$	$\omega/2\theta$
θ range (°)	2–25	2–22
No. reflections measured	5676	3942
No. unique reflections ($I > 2\sigma(I)$)	3692	2599
No. refined parameters	307	273
R	3.5	5.3
R_w	5.0	6.2
$GOF = [\Sigma w(k\lvert F_o\rvert - \lvert F_c\rvert)^2/(N_o - N_v)]^{1/2}$	1.436	1.354
Highest residual peak (e/Å^3)	0.85	0.79

TABLE 2. Fractional coordinates and equivalent isotropic thermal parameters of α-$[Bu_4N]_2[Ni(dsit)_2]_2$ (e.s.d.s in parentheses)

Atom	x/a	y/b	z/c	B_{iso} (Å^2)
Ni	0.95295(6)	0.60692(6)	0.07281(9)	3.24(2)
Se1	0.96043(6)	0.76927(5)	0.03577(9)	4.72(2)
Se2	1.08224(6)	0.60828(5)	0.28061(7)	3.88(2)
Se3	0.77441(6)	0.62963(5)	−0.05130(8)	4.29(2)
Se4	0.94173(5)	0.45009(5)	0.12383(7)	3.23(1)
S1	1.1505(2)	0.8915(1)	0.1663(2)	4.94(5)
S2	1.2597(2)	0.7511(1)	0.3641(2)	4.64(4)
S3	1.3590(2)	0.9305(2)	0.3522(3)	6.05(6)
S4	0.7388(1)	0.3320(1)	0.0427(2)	4.10(4)
S5	0.6031(1)	0.4830(2)	−0.1185(2)	4.64(4)
S6	0.5165(2)	0.2978(2)	−0.1079(3)	6.27(5)
C1	1.0867(5)	0.7881(5)	0.1671(7)	4.1(2)
C2	1.1390(5)	0.7245(5)	0.2610(7)	3.6(1)
C3	1.2614(6)	0.8614(5)	0.2986(8)	4.2(2)
C4	0.7949(5)	0.4377(5)	0.0386(7)	3.4(1)
C5	0.7309(5)	0.5102(5)	−0.0340(7)	3.6(1)
C6	0.6158(5)	0.3663(5)	−0.0624(7)	4.2(2)
N	0.2508(4)	0.2285(4)	0.5234(5)	3.7(1)
C10	0.2695(6)	0.3240(5)	0.6051(7)	4.0(2)
C11	0.2103(7)	0.4140(5)	0.5299(8)	4.9(2)
C12	0.2639(8)	0.5042(6)	0.6041(9)	5.9(2)
C13	0.3725(8)	0.5124(7)	0.561(1)	7.4(3)
C20	0.3147(6)	0.1451(5)	0.6109(7)	4.1(2)
C21	0.2725(7)	0.1356(6)	0.7499(8)	5.1(2)
C22	0.3521(8)	0.0523(6)	0.825(1)	6.5(2)
C23	0.3120(9)	0.0308(7)	0.962(1)	8.2(3)
C30	0.2938(5)	0.2186(5)	0.3817(7)	4.0(2)
C31	0.4147(6)	0.2384(5)	0.3927(8)	4.6(2)
C32	0.4592(6)	0.1930(6)	0.2620(8)	4.6(2)
C33	0.5783(6)	0.2154(6)	0.2632(9)	5.9(2)
C40	0.1247(5)	0.2278(6)	0.4942(9)	5.2(2)
C41	0.0923(6)	0.1320(7)	0.416(1)	6.9(2)
C42	−0.0392(7)	0.1488(9)	0.401(1)	12.5(3)
C43	−0.0926(9)	0.100(2)	0.305(2)	22.3(9)

Anisotropically refined atoms are given in the form of the isotropic equivalent displacement parameter defined as: $(4/3)[a^2B(1,1)+b^2B(2,2)+c^2B(3,3)+ab(\cos\gamma)B(1,2)+ac(\cos\beta)B(1,3)+bc(\cos\alpha)B(2,3)]$.

TABLE 3. Fractional coordinates and equivalent isotropic thermal parameters of β-$[Bu_4N]_2[Ni(dsit)_2]_2$ (e.s.d.s in parentheses). The letters A and B refer to two statistically occupied positions

Atom	x/a	y/b	z/c	B_{iso} (Å^2)
Ni	0.5380(1)	−0.0338(1)	−0.6586(2)	3.17(4)
Se1	0.4479(2)	−0.05981(9)	−0.8944(2)	5.08(4)
Se2	0.5974(1)	−0.19192(9)	−0.6345(2)	4.20(3)
Se3	0.5474(1)	0.10915(9)	−0.7242(1)	3.88(3)
Se4	0.6503(1)	−0.01369(8)	−0.4359(1)	3.46(3)
S1	0.3393(4)	−0.2296(3)	−1.0252(4)	7.0(1)
S2	0.4682(4)	−0.3452(3)	−0.8045(5)	7.1(1)
S3A	0.3300(7)	−0.4318(6)	−1.0401(9)	5.9(2)*
S3B	0.2612(8)	−0.4014(6)	−1.034(1)	6.7(2)*
S4	0.7826(3)	0.1480(3)	−0.3145(4)	4.8(1)
S5	0.6878(3)	0.2528(2)	−0.5565(4)	4.8(1)
S6	0.8380(4)	0.3321(3)	−0.3133(6)	7.5(1)
C1	0.432(1)	−0.1818(9)	−0.892(1)	4.4(3)*
C2	0.494(1)	−0.2329(8)	−0.788(1)	3.8(3)*
C3	0.363(1)	−0.333(1)	−0.962(2)	7.2(4)*
C4	0.693(1)	0.0985(8)	−0.451(1)	3.2(3)*
C5	0.651(1)	0.1470(8)	−0.564(1)	3.4(3)*
C6	0.773(1)	0.2492(9)	−0.392(1)	4.4(3)*
N	0.1701(9)	−0.7139(7)	−0.956(1)	4.5(3)
C10	0.108(1)	−0.6407(9)	−1.061(1)	4.5(4)
C11	0.179(1)	−0.630(1)	−1.170(1)	5.0(4)
C12	0.108(1)	−0.552(1)	−1.261(2)	5.3(4)
C13	0.168(2)	−0.540(1)	−1.381(2)	8.4(6)
C20	0.205(1)	−0.8102(8)	−1.035(2)	4.8(4)
C21	0.101(1)	−0.845(1)	−1.128(2)	6.9(5)
C22	0.157(2)	−0.943(1)	−1.196(2)	10.3(7)
C23A	0.091(3)	−1.001(3)	−1.262(4)	9(1)*
C23B	0.128(4)	−1.000(3)	−1.102(5)	11(1)*
C30	0.078(1)	−0.714(1)	−0.859(1)	5.7(4)
C31	0.123(2)	−0.783(1)	−0.743(2)	7.0(5)
C32	0.015(2)	−0.772(1)	−0.659(2)	10.3(6)
C33A	0.058(3)	−0.818(2)	−0.523(4)	7.4(9)*
C33B	0.032(3)	−0.863(3)	−0.569(4)	8(1)*
C40	0.287(1)	−0.6944(9)	−0.876(1)	4.6(4)
C41	0.272(1)	−0.603(1)	−0.781(2)	6.3(5)
C42	0.395(2)	−0.597(1)	−0.702(2)	11.6(7)
C43A	0.424(3)	−0.534(2)	−0.603(4)	8(1)*
C43B	0.472(3)	−0.592(2)	−0.767(3)	5.9(7)*

Starred atoms were refined isotropically. Anisotropically refined atoms are given in the form of the isotropic equivalent displacement parameter defined as: $(4/3)[a^2B(1,1)+b^2B(2,2)+c^2B(3,3)+ab(\cos\gamma)B(1,2)+ac(\cos\beta)B(1,3)+bc(\cos\alpha)B(2,3)]$.

factors for all atoms were taken from the International Tables for X-Ray Crystallography [20]. All calculations were performed on a VAX 11/730 computer.

Results and discussion

Description of the crystal structures

Large thermal motion is often observed at the end of aliphatic chains and can sometimes be analysed in terms of crystal disorder. For the α-phase, the very high anisotropy of the U tensors of the terminal atoms C(42) and C(43) of one of the butyl groups (see 'Supplementary material') indicates some degree of disorder. This is reflected by the high value of the equivalent isotropic thermal parameters (Table 2). No attempt was made to solve this disorder. For the β-phase, however, the disorder is more pronounced: the terminal atoms of three butyl groups of the Bu_4N^+ cation were observed in the difference Fourier maps as split, fuzzy peaks. Therefore, these atoms were considered statistically disordered over two positions (*vide supra*). The occupation factors were estimated to be 50–50% on the basis of the electron-density residues of the difference Fourier maps. More surprisingly, the terminal sulfur atom S(3) of one of the dsit ligands is also disordered and was treated in the same way. Distances between the refined disordered positions range from 0.85 to 1.81 Å (see 'Supplementary material'); such distances justify the use of a statistical

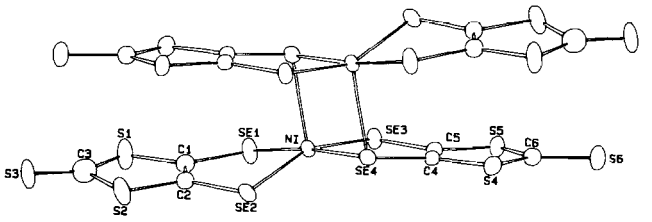

Fig. 1. The $[Ni(dsit)_2]_2^{2-}$ anion of the α- and β-phase. Thermal ellipsoids are drawn at 20% probability level.

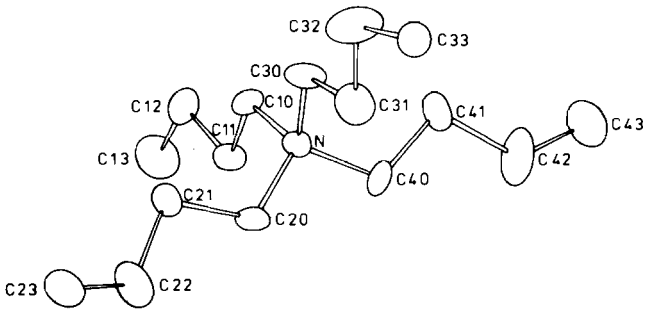

Fig. 2. The $[Bu_4N]^+$ cation of the α- and β-phase. Thermal ellipsoids are drawn at 20% probability level. Hydrogen atoms are omitted for clarity.

model to account for the features of the observed electron density distribution.

Tables 4 and 5 list all relevant bond distances and bond angles for the anions in both structures. The nickel atom lies in a distorted square pyramidal environment of five selenium donor atoms. Four equatorial atoms belong to the two dsit ligands of one $[Ni(dsit)_2]$ unit. The apical selenium atom belongs to a centrosymmetrically related $[Ni(dsit)_2]$ molecule. $[Ni(dsit)_2]_2$ dimers are thus formed through two Ni–Se bonds (see Fig. 1), as found in all other $Ni(dsit)_2$ compounds possessing a formal charge of -1 or -0.5 [10, 11]. The apical Ni–Se distance in the α- and β-phase (2.48 and 2.47 Å, respectively) is slightly but significantly longer than the equatorial bond lengths (Tables 4 and 5), which range from 2.316 to 2.347 Å. These apical Ni–Se bond distances are similar to the bond lengths found in $[Et_4N]_2[Ni(dsit)_2]_2$ [13], but shorter than those in the mixed-valence salts $[Me_4N][Ni(dsit)_2]_2$ and $[Me_4P][Ni(dsit)_2]_2$ [11, 13].

In both cases the individual $[Ni(dsit)_2]$ units are not planar; while one dsit ligand is nearly planar, the second one is puckered and twisted out of the plane of the former (see Table 6). The nickel atom lies almost in the plane of the planar dsit ligand. The spacing between the least-square mean planes through each $[Ni(dsit)_2]$ unit is 3.34 Å within a dimer in the α-phase, and 3.29 Å within a dimer in the β-phase (see Table 7).

As can be seen from Tables 4 and 5, the intramolecular distances and angles in the α- and β-structure differ only very slightly. The main difference between the two structures is the disorder discussed above. The overall orientation of the Bu_4N^+ groups in the lattice of the β-phase differs from that in the α-compound. As a result, the packing of the molecules in both crystal lattices is also slightly different (see Figs. 3 and 4).

Due to the bulky cations, the anionic dimers are perfectly isolated from each other. No significant interdimer contacts, normally responsible for the formation of a conduction band, exist, and therefore the electrical conductivity of these salts must be low.

TABLE 4. Selected bond distances (Å) and angles (°) for α-$[Bu_4N]_2[Ni(dsit)_2]_2$

Ni–Se1	2.347(1)	S2–C2	1.722(7)
Ni–Se2	2.336(1)	S2–C3	1.717(8)
Ni–Se3	2.317(1)	S3–C3	1.652(7)
Ni–Se4	2.316(1)	S4–C4	1.733(7)
Ni–Se4^i	2.480(1)	S4–C6	1.704(8)
Se1–C1	1.874(8)	S5–C5	1.735(7)
Se2–C2	1.902(7)	S5–C6	1.737(8)
Se3–C5	1.861(7)	S6–C6	1.654(7)
Se4–C4	1.892(6)	C1–C2	1.33(1)
S1–C1	1.753(7)	C4–C5	1.35(1)
S1–C3	1.730(8)		
Se1–Ni–Se2	92.59(4)	S1–C3–S3	123.4(5)
Se1–Ni–Se3	86.94(4)	S2–C3–S3	124.2(5)
Se1–Ni–Se4	176.15(5)	Se4–C4–S4^i	122.0(4)
Se1–Ni–Se4^i	91.75(4)	Se4–C4–C5	120.8(5)
Se2–Ni–Se3	152.93(5)	S4–C4–C5	117.1(5)
Se2–Ni–Se4	85.47(4)	Se3–C5–S5	120.9(4)
Se2–Ni–Se4^i	106.69(4)	Se3–C5–C4	124.2(5)
Se3–Ni–Se4	93.27(4)	S5–C5–C4	114.9(5)
Se3–Ni–Se4^i	100.37(4)	S4–C6–S5	113.1(4)
Se4–Ni–Se4^i	91.99(4)	S4–C6–S6	124.7(5)
Ni–Se4–Ni	88.01(4)	S5–C6–S6	122.2(5)
C1–S1–C3	97.7(4)	S2–C2–C1	117.8(6)
C2–S2–C3	97.6(4)	S1–C3–S2	112.3(4)
C4–S4–C6	97.3(4)	S1–C1–C2	114.5(6)
C5–S5–C6	97.6(3)	Se2–C2–S2	121.1(4)
Se1–C1–S1	120.7(5)	Se2–C2–C1	121.1(5)
Se1–C1–C2	124.7(5)		

^{i}represents the operation $(2-x, 1-y, -z)$.

Cyclic voltammetry

Due to the low solubility of $[Bu_4N]_2[Ni(dsit)_2]_2$ in acetonitrile, the measurements were carried out in acetone. Solutions of 0.1 M $[Bu_4N]_2[Ni(dsit)_2]_2$ in acetone show a reversible first wave (peak A1, C1 in Fig. 5(a)), corresponding to the $2[Ni(dsit)_2]^{2-}/[Ni(dsit)_2]_2^{2-}$ couple, at $E_{1/2} = -0.12$ V versus 0.1 N Ag/AgCl (reaction (1) in Scheme 2). This reaction formally corresponds

TABLE 5. Selected bond distances (Å) and angles (°) for β-$[Bu_4N]_2[Ni(dsit)_2]_2$

Ni–Se1	2.334(2)	S2–C3	1.77(2)
Ni–Se2	2.344(2)	S3A–S3B	0.85(1)
Ni–Se3	2.335(2)	S3A–C3	1.67(2)
Ni–Se4	2.317(2)	S3B–C3	1.75(2)
Ni–Se4^i	2.472(2)	S4–C4	1.73(1)
Se1–C1	1.88(1)	S4–C6	1.74(1)
Se2–C2	1.87(1)	S5–C5	1.73(1)
Se3–C5	1.89(1)	S5–C6	1.70(1)
Se4–C4	1.89(1)	S6–C6	1.64(1)
S1–C1	1.72(1)	C1–C2	1.33(2)
S1–C3	1.67(2)	C4–C5	1.33(2)
S2–C2	1.76(1)		
Se2–C2–S2	121.3(7)	Se2–C2–C1	124(1)
S1–C3–S2	113(1)	S2–C2–C1	114(1)
Se1–Ni–Se2	91.45(7)	S1–C3–S3A	131(1)
Se1–Ni–Se3	85.81(7)	S1–C3–S3B	117(1)
Se1–Ni–Se4	172.6(1)	S2–C3–S3A	114(1)
Se1–Ni–Se4^i	93.80(8)	S2–C3–S3B	128(1)
Se2–Ni–Se3	156.92(9)	Se2–Ni–Se4	86.58(7)
Se4–C4–S4^i	122.2(7)		
Se2–Ni–Se4^i	105.19(7)	Se4–C4–C5	122(1)
Se3–Ni–Se4	93.21(7)	S4–C4–C5	116(1)
Se3–Ni–Se4^i	97.86(7)	Se3–C5–S5	119.6(7)
Se4–Ni–Se4^i	93.60(7)	Se3–C5–C4	123(1)
C1–S1–C3	97.5(8)	S5–C5–C4	117(1)
C2–S2–C3	96.2(7)	S4–C6–S5	112.5(8)
S4–C6–S6	123.2(8)		
S5–C6–S6	124.2(9)		
C4–S4–C6	97.3(6)		
C5–S5–C6	97.7(6)		
Se1–C1–S1	120.5(8)		
Se1–C1–C2	121(1)		
S1–C1–C2	119(1)		

^{i}represents the operation $(1-x, -y, -1-z)$.

TABLE 6. Deviations (Å) of atoms from their least-squares plane. Starred atoms were not included in the calculations

Atoms	α-phase Plane I	β-phase Plane III
Se1	0.049	0.001
Se2	−0.021	−0.013
S1	−0.037	0.009
S2	0.036	0.019
S3	0.015	
C1	−0.030	−0.001
C2	−0.007	0.009
C3	−0.006	−0.025
Ni*	0.496	−0.634
	Plane II	Plane IV
Se3	−0.011	−0.018
Se4	0.064	−0.061
S4	−0.055	0.049
S5	0.028	0.000
S6	0.029	−0.049
C4	−0.033	0.039
C5	−0.026	0.041
C6	0.038	0.000
Ni*	0.057	0.047
Dihedral angle (°)	I–II	III–IV
	13.9	10.4

$$2[Ni(dsit)_2]^{2-} \longleftrightarrow [Ni(dsit)_2]_2^{2-} + 2e^- (1e^-/\text{mole } Ni(dsit)_2) \quad (1)$$

$$[Ni(dsit)_2]_2^{2-} \longrightarrow [Ni(dsit)_2]_2^{-} + 1e^- (0.5e^-/\text{mole } Ni(dsit)_2) \quad (2)$$

$$[Ni(dsit)_2]_2^{-} \longrightarrow [Ni(dsit)_2]^{-} + [Ni(dsit)_2]^0 (0e^-/\text{mole } Ni(dsit)_2) \quad (3)$$

$$2[Ni(dsit)_2]^0 + 1e^- \longrightarrow [Ni(dsit)_2]_2^{-} (0.5e^-/\text{mole } Ni(dsit)_2) \quad (4)$$

$$2[Ni(dsit)_2]^{-} \longrightarrow [Ni(dsit)_2]_2^{2-} (0e^-/\text{mole } Ni(dsit)_2) \quad (5)$$

$$[Ni(dsit)_2]_2^{-} + 1e^- \longrightarrow [Ni(dsit)_2]_2^{2-} (0.5e^-/\text{mole } Ni(dsit)_2) \quad (6)$$

Scheme 2.

to an Ni^{II}/Ni^{III} couple. A second peak which consists of an abrupt increase of the current intensity (anodic peak A2 at +0.183 V versus Ag/AgCl) may be attributed to the $[Ni(dsit)_2]_2^{2-}/[Ni(dsit)_2]_2^{-}$ couple (reaction (2) in Scheme 2). In fact, coulometry experiments carried out at constant potential (0.28 V), show that 0.5 electron per mole $Ni(dsit)_2$ has been exchanged during this oxidation step. The sudden increase of the current intensity is usually explained by assuming the deposition of a conducting species on the electrode during the oxidation process [21]. When reversing the scan at a switching potential of 0.4 V, two waves (peaks C2 and C2′, Fig. 5(a) at 0.08 and −0.01 V, respectively, are observed only in the reduction part of the cyclic voltammogram of $[Bu_4N]_2[Ni(dsit)_2]_2$.

As previously discussed by Hoyer and co-workers [22], the electrochemical data for $Ni(dsit)_2$, when compared to those for the $Ni(dmit)_2$ system, indicate that the $Ni^{II}(dsit)_2$ molecule is more difficult to oxidise to $Ni^{III}(dsit)_2$, but that further oxidation of $Ni^{III}(dsit)_2$ occurs relatively easier than the corresponding step for $Ni(dmit)_2$. Moreover, in acetone the reduction process of the highest oxidised $Ni(dsit)_2$ species takes place in two stages, as indicated by the splitting of the reduction wave (peaks C2 and C2′ in Fig. 5(a)). This splitting has not been previously observed in different solvents such as CH_3CN/DMF [22] and CH_3CN [10]. Such a large solvent-dependent redox behaviour for $[Bu_4N]_2[Ni(dsit)_2]_2$ is quite surprising, since the electrochemical properties of related systems, e.g., $M(dmit)_2$, hardly differ when changing from acetonitrile to acetone [21].

However, it should be noted that, when scanning from 0.40 V to increasing cathodic potentials (Fig. 5(b)), the first cathodic peak C2 at 0.08 V appears only when the switching potential is at least 0.20 V (curve 1 in Fig. 5(b)). The second reduction peak C2′ is observed

TABLE 7. Deviations (Å) of atoms from their least-squares mean plane

Atoms	α-phase Plane I	β-phase Plane II
Ni	0.392	0.365
Se1	0.156	−0.043
Se2	−0.299	−0.329
Se3	−0.002	0.129
Se4	0.473	0.474
S1	0.069	0.086
S2	−0.185	−0.180
S3	−0.020	
S4	0.071	0.046
S5	−0.184	−0.158
S6	−0.227	−0.229
C1	−0.025	−0.051
C2	−0.154	−0.182
C3	−0.057	0.045
C4	0.129	0.136
C5	−0.022	0.016
C6	−0.114	−0.125
D^a	I–I′	II–II′
	3.34	3.29

[a]Distance (Å) between the two centrosymmetrically related least-squares mean planes. Plane I′ is obtained by the $(2-x, 1-y, -z)$ symmetry operation on plane I. Plane II′ is obtained by the $(1-x, -y, -1-z)$ symmetry operation on plane II.

only when the switching potential is at least 0.23 V. Curve 3, which corresponds to a $-0.40 \rightarrow 0.25 \rightarrow -0.40$ V scan, clearly shows the two-step reduction process. This splitting may be explained by assuming that during the oxidation step at peak A2, after reaching a switching potential of at least 0.23 V, the thus formed $[Ni(dsit)_2]_2^-$ species dissociates into one $[Ni(dsit)_2]^-$ and one $[Ni(dsit)_2]^0$ species (Scheme 2). In this disproportionation-like reaction, there is no electron exchange. Hence, peak C2 may be attributed to the $2[Ni(dsit)_2]^0/[Ni(dsit)_2]_2^-$ couple (reaction (4), Scheme 2). The monoanionic monomer $[Ni(dsit)_2]^-$ rearranges to the dianionic dimer $[Ni(dsit)_2]_2^{2-}$ (reaction (5)). Peak C2′ corresponds to the reduction of the $[Ni(dsit)_2]_2^-$ dimer to the $[Ni(dsit)_2]_2^{2-}$ dimer.

Conclusions

It has been shown by single-crystal X-ray determinations that at least two modifications of $[Bu_4N]_2[Ni(dsit)_2]_2$ exist. Although they crystallise in different crystal habits, their structures differ only marginally. Furthermore, the α-phase appears to be thermodynamically more stable than the β-phase. Such a polymorphism is quite common in the mixed-valence dmit-based salts [3], and similarly, the stoichiometric salt $[Bu_4N][Ni(dmit)_2]$ was found to exist in two different crystal forms [23, 24].

Earlier single crystal X-ray measurements, performed by Hoyer and co-workers [22], show that there might exist yet another phase of the title compound. By comparing the unit-cell parameters, this phase was found to be isostructural with the monoclinic $[Bu_4N][Ni(dmit)_2]$ salt [23]. This result would indicate the existence of a monomeric $[Bu_4N][Ni(dsit)_2]$ phase. However, we could find no crystal possessing the cell dimensions reported by Hoyer and co-workers [22]. Recently, the crystal structure of $[Bu_4N][Ni(dsise)_2]$ (where dsise $= C_3S_2Se_3^{2-} =$ 1,3-dithiole-2-selenone-4,5-

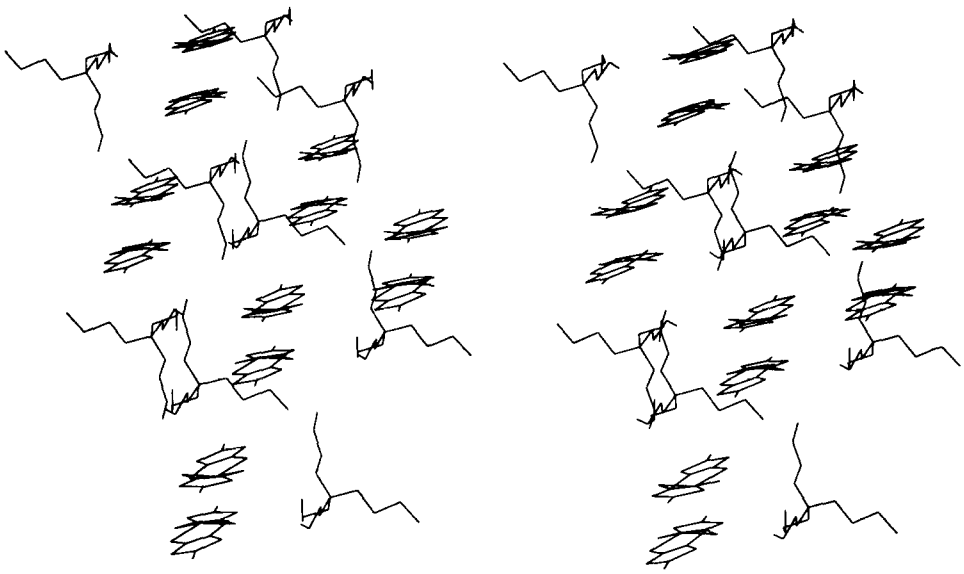

Fig. 3. Stereo view of the lattice of α-$[Bu_4N]_2[Ni(dsit)_2]_2$.

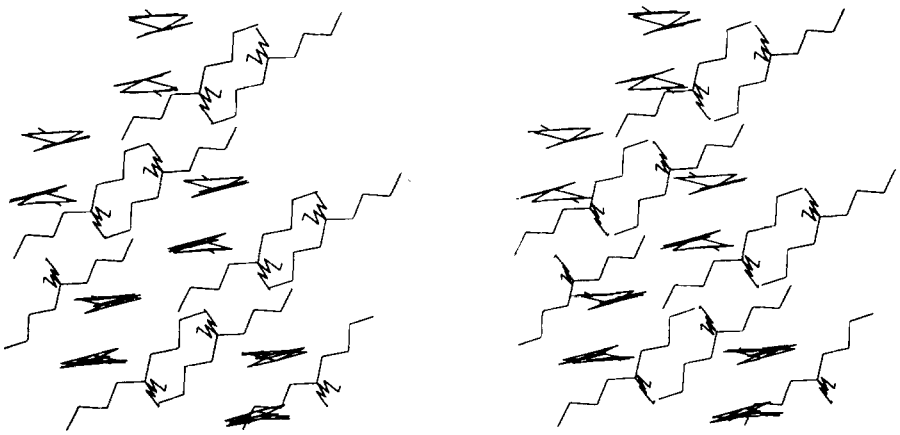

Fig. 4. Stereo view of the lattice of β-$[Bu_4N]_2[Ni(dsit)_2]_2$.

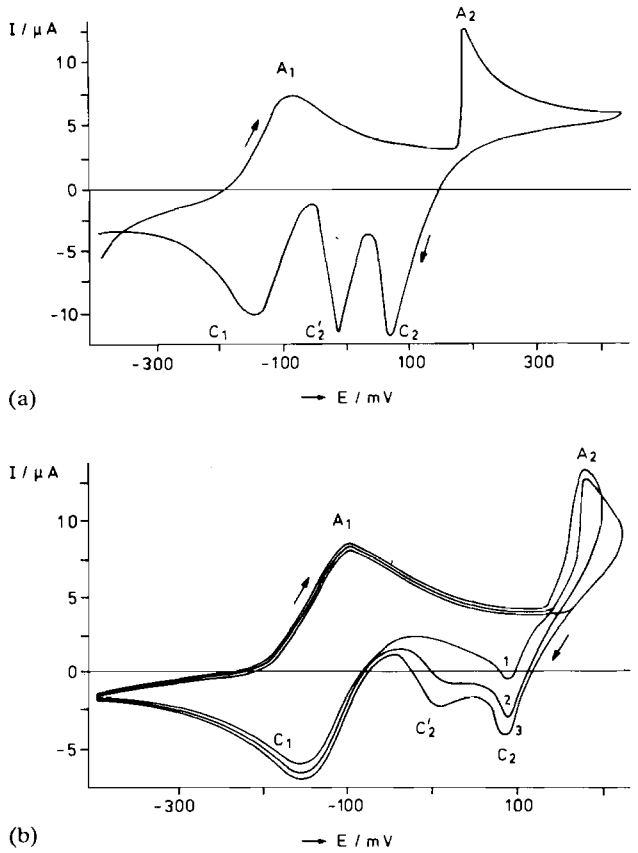

Fig. 5. (a) Cyclic voltammogram of $[Bu_4N]_2[Ni(dsit)_2]_2$ in acetone, $E_{inv} = 0.4$ V. (b) Effect of the value for E_{inv} on the cyclic voltammogram of $[Bu_4N]_2[Ni(dsit)_2]_2$ (see text for explanation of characters).

selenolate) was published [12], showing that in this salt the $Ni(dsise)_2$ units are not dimerised.

It is interesting to note that $[cation]_x[Ni(dsit)_2]$ mixed-valence salts have only been obtained in acetonitrile when the cations were small, i.e. Me_4N^+ and Me_4P^+, while no mixed-valence salts have been obtained when larger cations such as Et_4N^+ and Bu_4N^+ were used [13]. This may be due to the poor solubility of the $[Bu_4N]_2[Ni(dsit)_2]_2$ and $[Et_4N]_2[Ni(dsit)_2]_2$ dimers in acetonitrile. If a solution of $[R_4N]_2[Ni(dsit)_2]$ (with R = Bu or Et) in acetonitrile is electrochemically oxidised, the dimeric $[R_4N]_2[Ni(dsit)_2]_2$ compound crystallises on the anode as soon as it is formed and cannot be further oxidised to a fractional oxidation state. Choosing other solvents, e.g. acetone, should yield mixed-valence compounds with larger cations such as Bu_4N^+. This is suggested by the features in the cyclic voltammogram of $[Bu_4N]_2[Ni(dsit)_2]_2$ (see Fig. 5), which are typical for the formation of a conducting species on the anode. These features were not observed in acetonitrile [10].

Supplementary material

Anisotropically refined non-hydrogen atom thermal parameters, hydrogen atom calculated positional and thermal parameters, full tables of bond distances and angles, as well as tables of calculated and observed structure factor amplitudes are available from the authors on request.

Acknowledgements

The authors are indebted to D. de Montauzon for performing the CV measurements, and Dr R. Hage for helpful discussions. Professor E. Hoyer is thanked for his cooperation. We are grateful to the CNRS (Centre National de la Recherche Scientifique) in Paris and to NWO (Nederlandse Stichting voor Wetenschappelijk Onderzoek) for financial support. This work was financed in part (J.P.C., J.G.H., J.R.) by WFMO (Werkgroep Fundamenteel Materialen Onderzoek). The work at Sandia National Laboratories was supported by the Office of Basic Energy Sciences, Division of Materials Science, US Department of Energy.

References

1 K. Hoiczer, O. Klein, S.-M. Huang, R. B. Kaner, K.-J. Fu, R. L. Whetten and F. Diederich, *Science, 252* (1991) 1154, and refs. therein.

2 J. M. Williams, A. J. Schultz, U. Geiser, K. D. Carlson, A. M. Kini, H. H. Wang, W.-K. Kwok, M.-H. Whangbo and J. E. Schirber, *Science, 252* (1991) 1501, and refs. therein.

3 P. Cassoux, L. Valade, H. Kobayashi, A. Kobayashi, R. A. Clark and A. E. Underhill, *Coord. Chem. Rev., 110* (1991) 115, and refs. therein.

4 (a) A. Kobayashi, H. Kim, Y. Sasaki, K. Murata, R. Kato and H. Kobayashi, *J. Chem. Soc., Faraday Trans., 86* (1990) 361; (b) A. Kobayashi, H. Kobayashi, A. Miyamoto, R. Kato, R. A. Clark and A. E. Underhill, *Chem. Lett.*, (1991) 2163.

5 A. Kobayashi, H. Kim, Y. Sasaki, R. Kato and H. Kobayashi, *Solid State Commun., 62* (1987) 57.

6 R. E. Peierls, *Quantum Chemistry of Solids,* Clarendon, New York, 1964.

7 (a) R.-M. Olk, W. Dietzsch, J. Mattusch, J. Stach, C. Nieke and E. Hoyer, *Z. Anorg. Allg. Chem., 544* (1987) 199; (b) G. Matsubayashi, K. Akiba and T. Tanaka, *J. Chem. Soc., Dalton Trans.,* (1990) 115; (c) G. Matsubayashi and A. Yokozawa, *J. Chem. Soc., Dalton Trans.,* (1990) 3013; (d) 3535.

8 (a) R.-M. Olk, B. Olk, J. Rohloff and E. Hoyer, *Z. Chem., 30* (1990) 445; (b) H. Kobayashi, R. Kato and A. Kobayashi, *Synth. Met., 42* (1991) 2495; (c) V. Y. Khodorkovskii, J. Keicberga, K. A. Balodis and O. Y. Neiland, *Izv. Akad. Nauk Latv. SSR, Ser. Khim.,* (1988) 120; (d) J. P. Cornelissen, D. Reefman, J. G. Haasnoot, A. L. Spek and J. Reedijk, *Recl. Trav. Chim. Pays-Bas, 110* (1991) 345.

9 P. J. Nigrey, B. Morosin and J. F. Kwak, in S. A. Wolf and V. Z. Kresin (eds), *Novel Superconductivity,* Plenum, New York, 1987, p. 171.

10 (a) P. J. Nigrey, *Synth. Met., 27* (1988) B365; (b) B. Morosin and P. J. Nigrey, *Acta Crystallogr., Sect. A, 43* (1987) C130.

11 M. A. Beno, A. M. Kini, U. Geiser, H. H. Wang, K. D. Carlson and J. M. Williams, in G. Saito and S. Kagoshima (eds.), *The Physics and Chemistry of Organic Superconductors,* Springer, Berlin, 1990, p. 369.

12 R.-M. Olk, B. Olk, J. Rohloff, J. Reinhold, J. Sieler, K. Trübenbach, R. Kirmse and E. Hoyer, *Z. Anorg. Allg. Chem., 609* (1992) 103.

13 A. M. Kini, M. A. Beno, S. Budz, H. H. Wang and J. M. Williams, *Materials Research Society Symp. Proc., 173* (1990) 177.

14 O. Hönigschmid and W. Kapfenberger, *Z. Anorg. Allg. Chem., 212* (1933) 198.

15 G. Steimecke, H. Sieler, R. Kirmse and E. Hoyer, *Phosphorus Sulfur, 7* (1979) 49.

16 P. Cassoux, R. Dartiguepeyron, P.-L. Fabre and D. de Montauzon, *Actual. Chim.,* (1985) 79.

17 P. Cassoux, R. Dartiguepeyron, P.-L. Fabre and D. de Montauzon, *Electrochim. Acta, 11* (1985) 1485.

18 G. M. Sheldrick, *SHELX-76,* a program for crystal structure solution, University of Cambridge, Cambridge, UK, 1976.

19 C. K. Fair, *MolEN,* structure solution procedures, Enraf-Nonius, Delft, Netherlands, 1990.

20 *International Tables for X-Ray Crystallography,* Vol. IV, Kynoch, Birmingham, UK, 1974.

21 (a) L. Valade, M. Bousseau and P. Cassoux, *Nouv. J. Chim., 9* (1985) 351; (b) L. Valade, P. Cassoux, A. Gleizes and L. V. Interrante, *J. Phys. (Paris), Colloq., 44* (1983) C3, 1183.

22 R.-M. Olk, A. Röhr, J. Sieler, K. Köhler, R. Kirmse, W. Dietzsch, E. Hoyer and B. Olk, *Z. Anorg. Allg. Chem., 577* (1989) 206.

23 O. Lindqvist, L. Andersen, J. Sieler, G. Steimecke and E. Hoyer, *Acta Chem. Scand., Ser. A, 33* (1979) 445.

24 D. Mentzafos, A. Hountas and A. Terzis, *Acta Crystallogr., Sect. C, 44* (1988) 1590.